PCCP

Accepted Manuscript

ROYAL SOCIETY OF CHEMISTRY

www.rsc.org/pccp

Flexible band gap tuning of hexagonal boron nitride sheets interconnected by acetylenic bonds

Hongyu Zhang,* Youhua Luo,* Xiaojuan Feng, Lixia Zhao and Meng Zhang

Department of Physics, East China University of Science and Technology, Shanghai 200237, China

Abstract

The energetic and electronic properties of acetylenic-bond-interconnected hexagonal boron nitride sheets (BNyne), in which the number of rows of BN hexagonal rings (denoted as BN width) between neighboring arrays of acetylenic linkages increases consecutively, have been explored by using the first-principles calculations. Depending on the spatial position of B/N atoms with respect to the acetylenic linkages, there are two different types of configurations. The band structure features and band gap evolutions of BNyne structures as a function of BN width can be categorized into two families, corresponding to two distinct types of configurations. Of particular interest, for both types of BNyne structures, the band gap variations exhibit odd-even oscillating behavior depending on the BN width, which is related to the different symmetries of acetylenic chains in the unit cell. These results suggest that the embedded linear acetylenic chains can provide more flexibility for manipulation of the atomic and electronic properties of hexagonal boron nitride. These sp-sp^2 hybrid structures might promise importantly potential applications for developing nanoscaled electronic and optoelectronic devices.

*To whom correspondence should be addressed. E-mail: zhanghongyu@ecust.edu.cn; yhluo@ecust.edu.cn

1. Introduction

The recent surge in graphene research has stimulated growing interest in the investigation of two-dimensional (2D) materials owing to the wealth of unusual physical properties and phenomena as well as diverse potential applications in many emerging technologies. Besides graphene, diverse non-carbon graphene-like materials, including transition metal dichalcogenides (MoS_2, WS_2, *etc.*),[1–3] group IV (SiC, GeC, Si, Ge, Sn, *etc.*),[4–8] III-V (h-BN, AlN, GaN, InN, BP, *etc.*),[8–11] II-VI (BeO, ZnO, ZnS, *etc.*)[12–14] compounds have also been extensively investigated. Among all these experimentally obtained or theoretically predicted materials, two-dimensional hexagonal boron nitride (h-BN) might be the most intensively studied layered material after graphene as it is the isoelectronic analog to graphene and shares very similar structural characteristics.[15,16] The structural similarities between graphene and BN allow them to form essentially seamlessly in-plane hybrid nanostructures with continuously tunable C:BN stoichiometry.[16] On the other hand, the most significant difference between these two isostructured materials lies in their electrical conductivity, since graphene behaves as a semimetal with zero band gap while BN is a wide band-gap semiconductor, which limits their practical applications in electronic devices.[17] Consequently, this wide gap can be bridged by combining graphene and BN to develop semiconducting hexagonal layered structures with varying stoichiometry, enabling the applications in building electronic nanodevices.[18,19] In experiment, monolayer BN and various hybrid graphene-BN materials with fully controlled concentration, spatial variation, and dimension of interfaces and domains have been realized.[20–22]

Apart from the non-carbon 2D materials mentioned above, very recently a series of 2D carbon-based allotropes with a skeleton of sp- and sp^2-hybridized carbon atoms, called graphynes, have been drawing tremendous attention.[23–33] An important feature of graphynes is that they contain acetylenic linkages (−C≡C−) formed by sp-hybridized carbon atoms. Their lattice structures can be constructed by periodically replacing some selected sp^2-sp^2 covalent bonds in the frameworks of graphene with sp-sp acetylenic bonds.[34] Substitution designated at different sp^2-sp^2 bonds with different patterns leads to abundant structures of graphynes. The presence of acetylenic linkages in these 2D frameworks introduces a rich variation in electronic properties. For example, there exists a special class of graphyne substructures

associated with Dirac-cone-characterized electronic band structures in proximity of Fermi level, including α-graphyne, β-graphyne, δ-graphyne, and 6,6,12-graphyne.[34–40] On the other hand, in contrast to zero-band-gap graphene, graphyne and the already-synthesized graphdiyne have moderate band gaps,[29–32] which is quite crucial for the electronic applications. The natural band gaps originate from the inhomogeneous π-bindings between differently hybridized carbon atoms in these sp-sp^2 hybridized carbon networks.[41,42] Therefore, the presence of acetylenic linkages in graphynes provides extra flexibility in construction of their geometric structures and modulation of their electronic properties.[43,44]

Inspired by the flexibility of linear acetylenic linkages and the resulting diversity of the electronic properties of graphynes, we considered the possibilities of embedding acetylenic linkages to tune the electronic properties of hexagonal boron nitride sheets. In contrast to abundant efforts on sp^2-carbon-embedded BN, the studies of sp-carbon-embedded BN have rarely been reported up to now, and are therefore strongly desired. In this paper, we employed first-principles calculations within density functional theory (DFT)[45–50] to systematically study the electronic properties of hexagonal boron nitride periodically interconnected by acetylenic linkages. The number of rows of BN hexagonal rings between neighboring arrays of acetylenic linkages increases consecutively. By using a hybrid density functional which can predict the band gaps of materials with high accuracy, we found that the electronic properties of these sp-sp^2 hybrid structures are highly dependent on the number of rows of BN hexagons and their atomic arrangements with respect to the acetylenic linkages, indicating the flexible band gap tunability of hexagonal boron nitride induced by the acetylenic linkages. The present work is expected to promote the realization and applications of hexagonal boron nitride in nanoelectronics and nanodevices.

2. Methods and computational details

The structural relaxations and energy calculations were performed by using the DMol^3 package.[45,46] Generalized gradient approximation (GGA) in the form of the Perdew-Burke-Ernzerhof (PBE)[47] and the double numerical basis set plus polarization function (DNP) were selected for the spin-unrestricted DFT calculations. A vacuum region of 20 Å was applied in the *z*-direction to exclude mirror interactions between neighboring

images. The Brillouin zone (BZ) integrations were performed on a 6 × 3 ×1 Monkhorst−Pack *k*-point grid. The convergence tolerance of the energy was set to 10^{-5} Ha (1 Ha=27.2114 eV), and the maximum allowed force and displacement were 0.002 Ha/Å and 0.005 Å, respectively. To overcome the problem of band-gap underestimation in the GGA functionals, we employed the hybrid exchange-correlation functional Heyd-Scuseria-Ernzerhof (HSE06) (0.25 for the mixing constant and 0.11 $bohr^{-1}$ for the screening parameter)[48,49] implemented in CASTEP package[50] to calculate the band structures, which is better able to predict band gaps with high accuracy.[31] Based on the convergence test calculations, the energy cutoff of the plane wave basis set was set to 700 eV. The electronic structure calculations were carried out based on the optimized geometries from the DMol^3 calculations. As a check on the validity of our theoretical method, the band gap of diamond was calculated to be 5.39 eV with HSE06 functional, in good agreement with the experimental value of 5.45 eV.[51] Additionally, using the present theoretical strategy, the electronic properties of other graphyne-based allotropes have also been accurately predicted in our previous work.[36,41]

3. Results and discussion

For convenience, we characterized this series of acetylenic-bond-interconnected BN structures by the number of rows of BN hexagonal rings (denoted as BN width) between neighboring arrays of acetylenic linkages, and labeled them as *n*-BNyne, where *n* refers to the BN width and ranges from 1 to 10 for structures studied here. Depending on the spatial position of B/N atoms with respect to the acetylenic linkages, there are two different types of configurations, labeled as *n*-BNyne-Type I and *n*-BNyne-Type II, respectively. Four representative BNyne structures are illustrated in Fig. 1. Two ends of each acetylenic linkage connect with different types of atoms in Type I arrangement whereas with the same types of atoms in Type II arrangement. Our calculations show that the average lengths of C-B and C-N bonds in Type I configurations are 1.50 and 1.35 Å, respectively, while those in Type II configurations are 1.52 and 1.37 Å, respectively. As a result, for both C-B and C-N bonds, the lengths in Type I configurations are less than those in Type II configurations by about 0.02 Å. This indicates that interactions between these atoms are stronger in Type I configurations than those in Type II configurations, which is induced by more favorable charge transfer in the

former atomic arrangement than that in the latter one. The lengths of C-C bonds in the carbon chains were calculated to be 1.20~1.22 Å, demonstrating a triple bond associated with sp-hybridized carbon atoms.

To evaluate the energetic stability of BNyne structures, we calculated the cohesive energy by the formula: $E_{coh} = (m_B E_B + m_N E_N + m_C E_C - E_{BN/C})/m$, where E_B, E_N, E_C, and $E_{BN/C}$ are the total energies of free B, N, C atoms and BNyne systems, respectively, and m_B, m_N, and m_C are the numbers of B, N, and C atoms in the unit cell, respectively, while m is the total number of atoms in the unit cell. Fig. 2 gives the cohesive energy evolutions of two different types of BNyne structures as a function of BN width. From this figure, we can see the following features: (1) These BNyne structures are energetically less favorable than pristine BN sheet (E_{coh}=6.99 eV) and graphitic BC_2N monolayer with the most favorable atomic arrangement[52] (E_{coh}=7.13 eV). This is due to the presence of sp-hybridized atoms in BNyne structures. (2) The cohesive energies of these two types of BNyne structures increase monotonically with increasing BN width. This increasing relationship can be easily understood in terms of the fact that the ratio of sp^2-hybridized atoms to sp-hybridized atoms increases with increasing BN width. (3) BNyne-Type I is energetically more stable than BNyne-Type II with the same BN width. This is related to the favorability of charge transfer induced by the former arrangement over the latter one. Embedding carbon chains results in the charge redistribution mostly in the neighborhood of the carbon chains, while the charge distribution away from the interfaces approaches that of a perfect BN sheet. In view of different atomic electronegativities, the C atoms bonded to B atoms receive electrons, while C atoms bonded to N atoms lose electrons. Our Mulliken charge analysis reveals that the C atoms linked with B (N) atoms receive (lose) more electrons in Type I arrangement than those in Type II arrangement with the same BN width. To further confirm the stability of BNyne structures, we performed *ab initio* molecular dynamics (MD) simulations on the relatively most unfavorable 1-BNyne-Type II in a 5 × 2 supercell at 500 K for 1 ps by using the NVT ensemble implemented in CASTEP package. No obvious collapse tendency of the framework was found at this time scale. Furthermore, with the increase of BN width, the stability of BNyne structures will be greatly improved, indicated by the cohesive energy. These results imply the stability and plausibility of BNyne structures. Moreover, the most recent successful

synthesis of various hybrid BN-C materials[21,22] and extended-graphdiyne wires by vicinal surface templating[53] may also be helpful for the experimental realization of BNyne structures.

Next we explored the electronic properties of these BNyne structures by using HSE06 hybrid functional. Fig. 3 gives the band structures of BNyne structures represented by four samples (see ESI for more band structures). It can be seen that the electronic properties of BNyne structures sensitively depend on the atomic arrangements. The band structures of BNyne monolayers are separated into two different categories, corresponding to two types of BNyne configurations. BNyne-Type I structures are semiconductors with a direct band gap, located at Y and Γ point for structures with odd and even BN widths, respectively, which is crucial for the optoelectronic applications. By contrast, BNyne-Type II structures possess indirect band gaps. Detailed analysis demonstrates that for BNyne-Type II structures, the valence band maximum (VBM) locates at Γ point, while the conduction band minimum (CBM) locates at X and S point for odd and even widths, respectively. However, the band structures of Type II configurations with odd and even widths show no significant difference, since the lowest unoccupied band between X and S point is very flat. For both types of BNyne configurations, the direct/indirect band gap feature is intact regardless of BN width. Hence, the feature of band gap of BNyne structures is characterized by BN atomic arrangements with respect to the acetylenic chains.

We further investigated the band gap modulation of BNyne structures by varying the BN width, as shown in Fig. 4. It is interesting to note that the band gap evolution of these two types of BNyne structures versus BN width exhibits two opposite overall tendencies, with the band gaps lying in two distinct value ranges. Generally speaking, for BNyne-Type I structures, the band gaps increase as a function of increasing BN width, ranging from 2.187 eV for n=1 to 2.552 eV for n=10. By contrast, BNyne-Type II structures experience an overall decrease in the band gaps with increasing BN width, changing from 1.134 eV for n=1 to 0.837 eV for n=10. More interestingly, for both types of n-BNyne ($n \geq 4$) structures, the band gaps oscillate between odd and even BN widths, as shown in Fig. 4(b) and (c). Consequently, the band gaps of BNyne structures can be modulated by changing the BN width and its atomic arrangements with respect to the acetylenic chains. These results indicate that the embedded linear acetylenic chains provide more flexibility for band gap engineering in hexagonal boron

nitride. The tunable band gap of BNyne structures may find applications in nanoscaled electronic and optoelectronic devices.

To reveal the origin of the band gap and the BN width and arrangement dependence of BNyne structures, we plotted the electron density isosurfaces of the highest occupied valence band (HOVB) and the lowest unoccupied conduction band (LUCB) in Fig. 5. For BNyne-Type I structures, the HOVB is highly localized on the π orbitals of C≡C bonds and *p* orbitals of N atoms of C-N bonds, while the LUCB mainly originates from *p* orbitals of B atoms of C-B bonds, C atoms of C-N bonds, and B atoms of the BN hexagonal rings closest to the acetylenic chains. For BNyne-Type II structures, the spatial distribution of the HOVB is similar to that of BNyne-Type I, whereas the LUCB is mainly localized on the π orbitals of C-B bonds along the acetylenic chains. These results manifest that distinct trends of band gap variation as a function of BN width mentioned above mostly arise from the change of LUCB of these two types of BNyne structures, where top-to-top B atoms at the interfaces of BNyne-Type II structures lower down the energy of LUCB. Besides, the width dependent oscillatory behavior of the band gaps for both types of *n*-BNyne structures may be related to the different symmetries of acetylenic chains in the unit cell for the structures with odd and even BN widths.

4. Conclusions

In summary, based on first-principles calculations, we have systematically explored the electronic structures tunability of hexagonal boron nitride induced by the acetylenic linkages. The hybrid structures can be viewed as continuously increasing number of rows of BN hexagonal rings between neighboring arrays of acetylenic linkages (BNyne). Interestingly, the band structures and band gap evolutions as a function of BN width are separated into two categories, corresponding to two distinct BN atomic arrangements with respect to the acetylenic chains. For BNyne-Type I structures, the band gaps generally increase with the increase of BN width, whereas the band gaps of BNyne-Type II generally decrease with increasing BN width. For both types, the band gap variations exhibit odd-even oscillating behavior depending on the BN width. Therefore, the band gaps of BNyne structures can be modulated by changing the BN width and its atomic arrangements with respect to the

acetylenic chains. Such flexible modulation holds great promise for applications of these two-dimensional acetylenic-bond-interconnected BN structures in nanoscaled electronic and optoelectronic devices.

Acknowledgments

The author Hongyu Zhang is grateful to Dr. Tao He for useful discussions. This work was supported by the Fundamental Research Funds for the Central Universities (No. WM1214043), the National Natural Science Foundation of China (Nos. 11304096 and 11204079), and the Natural Science Foundation of Shanghai (No. 12ZR1407000).

References

1 S. Lebègue and O. Eriksson, *Phys. Rev. B*, 2009, **79**, 115409.

2 K. F. Mak, C. Lee, J. Hone, J. Shan and T. F. Heinz, *Phys. Rev. Lett.*, 2010, **105**, 136805.

3 Z. Y. Zhu, Y. C. Cheng and U. Schwingenschlögl, *Phys. Rev. B*, 2011, **84**, 153402.

4 S. Cahangirov, M. Topsakal, E. Aktürk, H. Şahin and S. Ciraci, *Phys. Rev. Lett.*, 2009, **102**, 236804.

5 J. C. Garcia, D. B. de Lima, L. V. C. Assali and J. F. Justo, *J. Phys. Chem. C*, 2011, **115**, 13242–13246.

6 C. Zhang, A. De Sarkar and R. Q. Zhang, *J. Phys. Chem. C*, 2011, **115**, 23682–23687.

7 B. Lalmi, H. Oughaddou, H. Enriquez, A. Kara, S. Vizzini, B. Ealet and B. Aufray, *Appl. Phys. Lett.*, 2010, **97**, 223109.

8 H. Şahin, S. Cahangirov, M. Topsakal, E. Bekaroglu, E. Akturk, R. T. Senger and S. Ciraci, *Phys. Rev. B*, 2009, **80**, 155453.

9 H. L. Zhuang, A. K. Singh and R. G. Hennig, *Phys. Rev. B*, 2013, **87**, 165415.

10 C. Jin, F. Lin, K. Suenaga and S. Iijima, *Phys. Rev. Lett.*, 2009, **102**, 195505.

11 M. Topsakal, E. Aktürk and S. Ciraci, *Phys. Rev. B*, 2009, **79**, 115442.

12 C. L. Freeman, F. Claeyssens, N. L. Allan and J. H. Harding, *Phys. Rev. Lett.*, 2006, **96**, 066102.

13 G. Weirum, G. Barcaro, A. Fortunelli, F. Weber, R. Schennach, S. Surnev and F. P. Netzer, *J. Phys. Chem. C*, 2010, **114**, 15432–15439.

14 M. Topsakal, S. Cahangirov, E. Bekaroglu and S. Ciraci, *Phys. Rev. B*, 2009, **80**, 235119.

15 S. Z. Butler, S. M. Hollen, L. Cao, Y. Cui, J. A. Gupta, H. R. Gutiérrez, T. F. Heinz, S. S. Hong, J. Huang, A. F. Ismach, E. Johnston-Halperin, M. Kuno, V. V. Plashnitsa, R. D. Robinson, R. S. Ruoff, S. Salahuddin, J. Shan, L. Shi, M. G. Spencer, M. Terrones, W. Windl and J. E. Goldberger, *ACS Nano*, 2013, **7**, 2898–2926.

16 Y. Lin and J. W. Connell, *Nanoscale*, 2012, **4**, 6908–6939.

17 S. Bhowmick, A. K. Singh and B. I. Yakobson, *J. Phys. Chem. C*, 2011, **115**, 9889–9893.

18 X. Fan, Z. Shen, A. Q. Liu and J. L. Kuo, *Nanoscale*, 2012, **4**, 2157–2165.

19 P. P. Shinde and V. Kumar, *Phys. Rev. B*, 2011, **84**, 125401.

20 K. K. Kim, A. Hsu, X. Jia, S. M. Kim, Y. Shi, M. Hofmann, D. Nezich, J. F.

Rodriguez-Nieva, M. Dresselhaus, T. Palacios and J. Kong, *Nano Lett.*, 2012, **12**, 161–166.

21 L. Ci, L. Song, C. Jin, D. Jariwala, D. Wu, Y. Li, A. Srivastava, Z. F. Wang, K. Storr, L. Balicas, F. Liu and P. M. Ajayan, *Nat. Mater.*, 2010, **9**, 430–435.

22 Y. Gong, G. Shi, Z. Zhang, W. Zhou, J. Jung, W. Gao, L. Ma, Y. Yang, S. Yang, G. You, R. Vajtai, Q. Xu, A. H. MacDonald, B. I. Yakobson, J. Lou, Z. Liu and P. M. Ajayan, *Nat. Commun.*, 2014, **5**, 3193.

23 R. H. Baughman, H. Eckhardt and M. Kertesz, *J. Chem. Phys.*, 1987, **87**, 6687–6699.

24 A. N. Enyashin and A. L. Ivanovskii, *Phys. Status Solidi B*, 2011, **248**, 1879–1883.

25 H. Zhang, X. He, M. Zhao, M. Zhang, L. Zhao, X. Feng and Y. Luo, *J. Phys. Chem. C*, 2012, **116**, 16634–16638.

26 G. Li, Y. Li, H. Liu, Y. Guo, Y. Li and D. Zhu, *Chem. Commun.*, 2010, **46**, 3256–3258.

27 X. Qian, H. Liu, C. Huang, S. Chen, L. Zhang, Y. Li, J. Wang and Y. Li, *Sci. Rep.*, 2015, **5**, 7756.

28 H. Zhang, Y. Xia, H. Bu, X. Wang, M. Zhang, Y. Luo and M. Zhao, *J. Appl. Phys.*, 2013, **113**, 044309.

29 M. Long, L. Tang, D. Wang, Y. Li and Z. Shuai, *ACS Nano*, 2011, **5**, 2593–2600.

30 G. Luo, X. Qian, H. Liu, R. Qin, J. Zhou, L. Li, Z. Gao, E. Wang, W. Mei, J. Lu, Y. Li and S. Nagase, *Phys. Rev. B*, 2011, **84**, 075439.

31 Y. Jiao, A. Du, M. Hankel, Z. Zhu, V. Rudolph and S. C. Smith, *Chem. Commun.*, 2011, **47**, 11843–11845.

32 H. Lu and S. Li, *J. Mater. Chem. C*, 2013, **1**, 3677–3680.

33 H. Zhang, M. Zhao, X. He, Z. Wang, X. Zhang and X. Liu, *J. Phys. Chem. C*, 2011, **115**, 8845–8850.

34 Z. Liu, G. Yu, H. Yao, L. Liu, L. Jiang and Y. Zheng, *New J. Phys.*, 2012, **14**, 113007.

35 H. Huang, W. Duan and Z. Liu, *New J. Phys.*, 2013, **15**, 023004.

36 A. Wang, L. Li, X. Wang, H. Bu and M. Zhao, *Diamond Relat. Mater.*, 2014, **41**, 65–72.

37 D. Malko, C. Neiss and A. Görling, *Phys. Rev. B*, 2012, **86**, 045443.

38 D. Malko, C. Neiss, F. Viñes and A. Görling, *Phys. Rev. Lett.*, 2012, **108**, 086804.

39 B. G. Kim and H. J. Choi, *Phys. Rev. B*, 2012, **86**, 115435.

40 M. Zhao, W. Dong and A. Wang, *Sci. Rep.*, 2013, **3**, 3532.

41 H. Bu, M. Zhao, H. Zhang, X. Wang, Y. Xi and Z. Wang, *J. Phys. Chem. A*, 2012, **116**, 3934–3939.

42 X. He, J. Tan, H. Bu, H. Zhang and M. Zhao, *Chin. Sci. Bull.*, 2012, **57**, 3080.

43 N. B. Singh, B. Bhattacharya and U. Sarkar, *Struct. Chem.*, 2014, **25**, 1695–1710.

44 Y. Ding and Y. Wang, *Nanoscale Res. Lett.*, 2015, **10**, 13.

45 B. Delley, *J. Chem. Phys.*, 1990, **92**, 508–517.

46 B. Delley, *J. Chem. Phys.*, 2000, **113**, 7756–7764.

47 J. P. Perdew, K. Burke and M. Ernzerhof, *Phys. Rev. Lett.*, 1996, **77**, 3865–3868.

48 J. Heyd, G. E. Scuseria and M. Ernzerhof, *J. Chem. Phys.*, 2003, **118**, 8207–8215.

49 A. V. Krukau, O. A. Vydrov, A. F. Izmaylov and G. E. Scuseria, *J. Chem. Phys.*, 2006, **125**, 224106.

50 S. J. Clark, M. D. Segall, C. J. Pickard, P. J. Hasnip, M. J. Probert, K. Refson and M. C. Payne, *Zeitschrift fuer Kristallographie*, 2005, **220**, 567–570.

51 L. A. Chernozatonskii, P. B. Sorokin, A. G. Kvashnin and D. G. Kvashnin, *JETP Lett.*, 2009, **90**, 134–138.

52 A. Y. Liu, R. M. Wentzcovitch and M. L. Cohen, *Phys. Rev. B*, 1989, **39**, 1760–1765.

53 B. Cirera, Y. Q. Zhang, J. Björk, S. Klyatskaya, Z. Chen, M. Ruben, J. V. Barth and F. Klappenberger, *Nano Lett.*, 2014, **14**, 1891–1897.

Figure Captions:

Fig. 1 Representative illustrations of two types of BNyne structures. (a) 1-BNyne-Type I, (b) 2-BNyne-Type I, (c) 1-BNyne-Type II, and (d) 2-BNyne-Type II. The dashed rectangle denotes a unit cell.

Fig. 2 Cohesive energy evolutions of two different types of BNyne structures as a function of BN width.

Fig. 3 Band structures of (a) odd-BNyne-Type I structures represented by 1-BNyne-Type I, (b) even-BNyne-Type I structures represented by 2-BNyne-Type I, (c) odd-BNyne-Type II structures represented by 1-BNyne-Type II, and (d) even-BNyne-Type II structures represented by 2-BNyne-Type II. The Brillouin zone with high symmetric points is shown in the inset of (a). The horizontal dash-dot lines indicate the Fermi level.

Fig. 4 (a) Energy band gap evolutions of two distinct types of BNyne structures as a function of BN width. For clarity, the band gap variations of (b) BNyne-Type I and (c) BNyne-Type II are also plotted separately.

Fig. 5 The isosurfaces of the electron density of the highest occupied valence band (HOVB) and the lowest unoccupied conduction band (LUCB) of BNyne structures represented by four samples. (a) 4-BNyne-Type I, (b) 5-BNyne-Type I, (c) 4-BNyne-Type II, and (d) 5-BNyne-Type II. The isovalue is 0.03 e/Å^3.

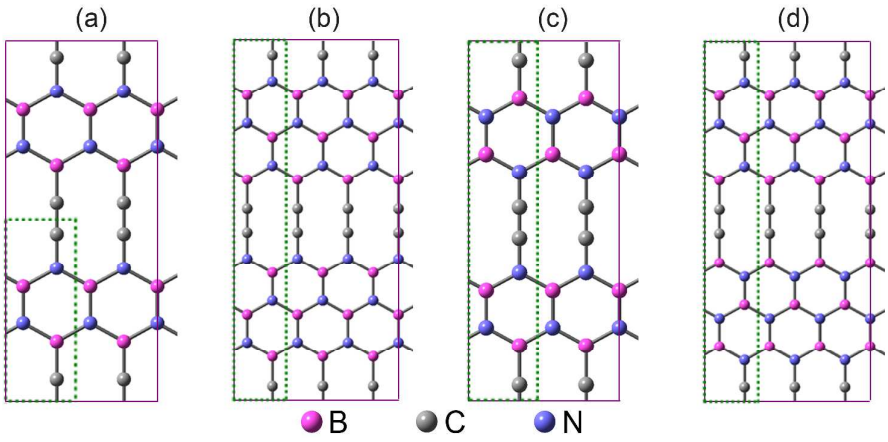

Fig. 1 Representative illustrations of two types of BNyne structures. (a) 1-BNyne-Type I, (b) 2-BNyne-Type I, (c) 1-BNyne-Type II, and (d) 2-BNyne-Type II. The dashed rectangle denotes a unit cell.

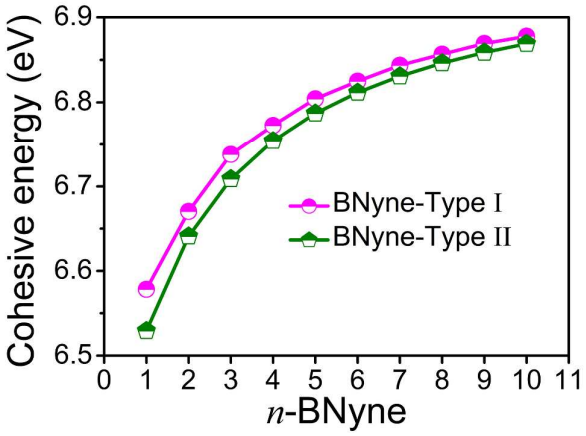

Fig. 2 Cohesive energy evolutions of two different types of BNyne structures as a function of BN width.

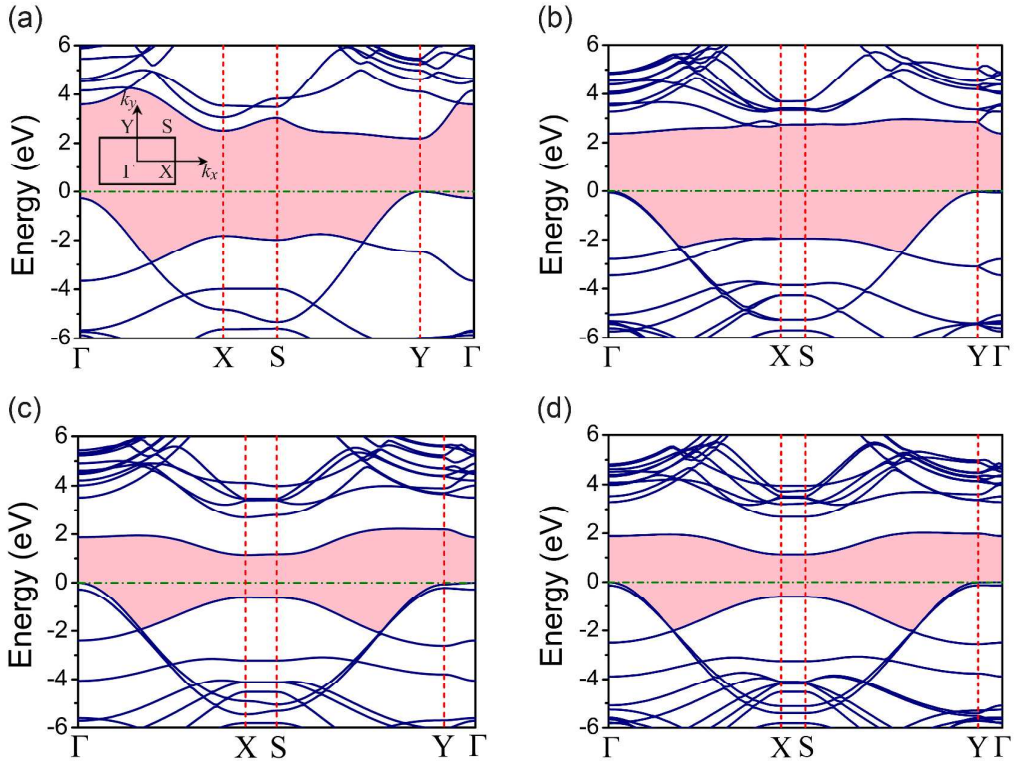

Fig. 3 Band structures of (a) odd-BNyne-Type I structures represented by 1-BNyne-Type I, (b) even-BNyne-Type I structures represented by 2-BNyne-Type I, (c) odd-BNyne-Type II structures represented by 1-BNyne-Type II, and (d) even-BNyne-Type II structures represented by 2-BNyne-Type II. The Brillouin zone with high symmetric points is shown in the inset of (a). The horizontal dash-dot lines indicate the Fermi level.

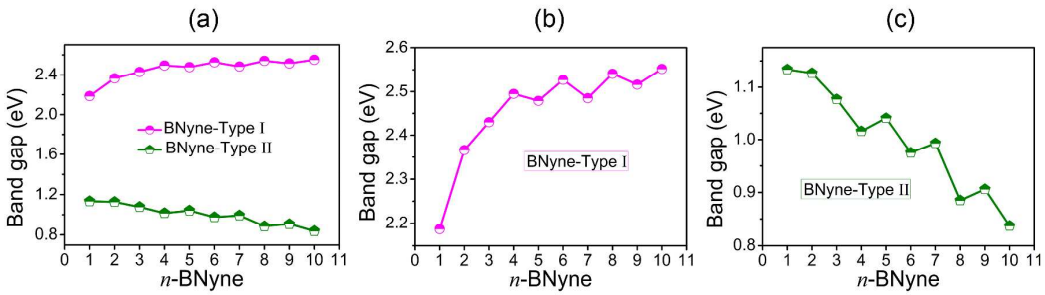

Fig. 4 (a) Energy band gap evolutions of two distinct types of BNyne structures as a function of BN width. For clarity, the band gap variations of (b) BNyne-Type I and (c) BNyne-Type II are also plotted separately.

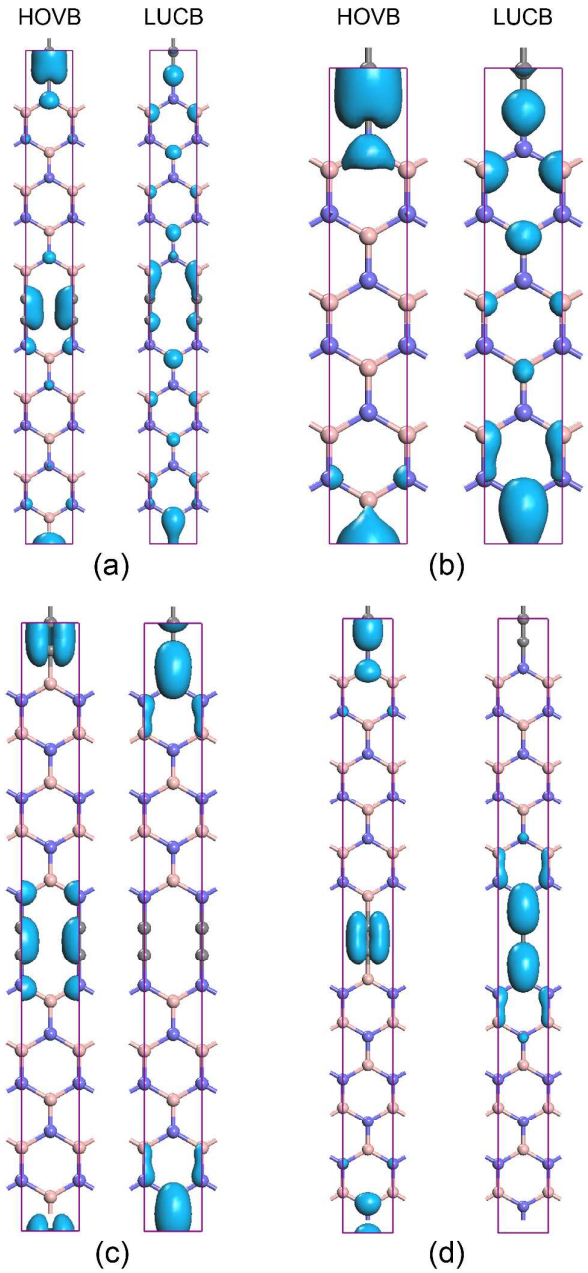

Fig. 5 The isosurfaces of the electron density of the highest occupied valence band (HOVB) and the lowest unoccupied conduction band (LUCB) of BNyne structures represented by four samples. (a) 4-BNyne-Type I, (b) 5-BNyne-Type I, (c) 4-BNyne-Type II, and (d) 5-BNyne-Type II. The isovalue is 0.03 e/Å^3.

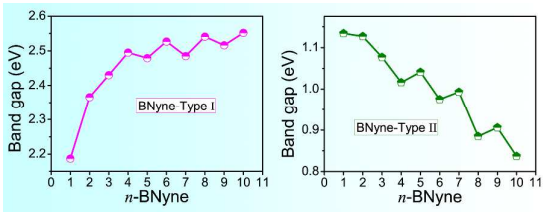

Table of Contents Image